J. Electrochem. Sci. Eng. **16** (2026) 3213; https://doi.org/10.5599/jese.3213

Open Access : : ISSN 1847-9286

www.jESE-online.org

Original scientific paper

Sm/UiO-66 metal organic framework modified electrode for the electrochemical determination of ethambutol hydrochloride in pharmaceutical formulations and human urine

Pham Thi Huyen Thoa[1,2], Nguyen Quang Man[3], Phan Tu Quy[2,✉], Nguyen Chi Bao[4], Le Van Thanh Son[5], Le Lam Son[1], Dao Ngoc Nhiem[6,✉] and Dinh Quang Khieu[1,✉]

[1]*University of Sciences, Hue University, Vietnam*
[2]*Department of Natural Sciences & Technology, Tay Nguyen University, Vietnam*
[3]*University of Medicine and Pharmacy, Hue University, Vietnam*
[4]*Department of Science, Technology and International Relations, Hue University, Vietnam*
[5]*University of Education and Technology, The University of Danang, Vietnam*
[6]*Institute of Materials Science, Vietnam Academy of Science and Technology, 18 Hoang Quoc Viet Street, Nghia Do, Hanoi, Vietnam*

Corresponding Authors: ✉phantuquy@ttn.edu.vn; ✉nhiemdn@ims.vast.ac.vn; ✉dqkhieu@hueuni.edu.vn

Received: January 12, 2026; Accepted: February 16, 2026; Published: February 25, 2026

Abstract

In this study, a samarium-modified metal-organic framework, Sm/UiO-66, was synthesized and used as an electrode modifier for detecting ethambutol hydrochloride. The material was characterized by X-ray diffraction, Fourier-transform infrared spectroscopy, electrochemical impedance spectroscopy, energy-dispersive X-ray mapping, X-ray photoelectron spectroscopy and scanning electron microscopy. The electrochemical behaviour of ethambutol at the Sm/UiO-66 modified glassy carbon electrode was examined using cyclic voltammetry and differential pulse voltammetry. The Sm/UiO-66-modified electrode exhibited a strong electrocatalytic response toward ethambutol oxidation, with a clearly defined anodic peak current. Under optimized conditions, the sensor showed a linear response in the 0.5 to 9.9 µM concentration range with a detection limit of 0.23 µM. The sensor demonstrated excellent repeatability (RSD < 3.5 %, n = 10), stability over one week, and high selectivity against common interfering substances. Notably, the proposed method was successfully applied to determine ethambutol in three pharmaceutical and three human urine samples, with exceptional recoveries. The proposed Sm/UiO-66 modified electrode is a reliable, sensitive, and selective tool for ethambutol analysis. This method can serve as a practical alternative or complementary approach for routine pharmaceutical quality control and therapeutic monitoring in tuberculosis treatment.

Keywords
Electrochemical sensor; modified glassy carbon; samarium doping; ethambutol detection; real sample analysis.

Introduction

Tuberculosis (TB) remains a major global health challenge, especially in developing countries. It today causes 1.3 million deaths yearly, mostly in low and middle-income countries [1]. Ethambutol hydrochloride (ETB) is a first-line antitubercular agent and helps prevent resistance to other first-line anti-TB agents, such as rifampicin [2]. ETB is usually administered as the hydrochloride (HCl) salt at a recommended dose of 15-25 mg kg^{-1} [2]. Precise dosing of ETB is of critical importance: while insufficient levels can lead to therapeutic failure and drug resistance, excessive or prolonged use is associated with serious adverse effects such as loss of visual acuity, red-green color blindness, and in some cases irreversible vision damage [3,4], gastrointestinal discomfort (nausea, vomiting, abdominal pain) [5]. These concerns highlight the need for sensitive, rapid analytical techniques to monitor ETB content in pharmaceutical formulations and ensure efficacy and patient safety.

Available analytical methods for ETB detection, such as reversed-phase liquid chromatography coupled with nano-quantity analyte detector [6], sensitive fluorescent probes [7], and liquid chromatography-tandem mass spectrometry [8], provide acceptable accuracy but often require complex operation and instrumentation, labor-intensive sample preparation, or high operational costs. In this regard, electrochemical methods have been recognized as potential alternatives owing to their inherent advantages, including high sensitivity, low detection limits, rapid response, and cost-effectiveness [9]. However, the performance of such electrochemical sensors depends significantly on electrode modifiers, including surface area, electrocatalytic sites, and their ability to enhance electron transfer.

Metal-organic frameworks (MOFs), a class of porous crystalline materials made of metal clusters and organic linkers, have recently gained increasing attention for sensor development [10]. Among these, UiO-66, a zirconium-based MOF or UiO-66-based materials [11,12], has shown potential as an electrode modifier for developing electrochemical sensors for the rapid detection of manganese ions [13], dopamine in human serum [14], and morphine and tramadol [15] due to their high chemical and thermal stability, tunable porosity, and ease of functionalization. Samarium oxide (Sm_2O_3), a rare-earth sesquioxide with high permittivity, is used in dielectric resonators, capacitors, and resistance-based gas sensors [16]. Samarium (Sm), with its unique redox activity [17,18], can enhance charge-transfer kinetics, making it favorable for electrochemical systems [19]. Incorporating samarium into MOFs has been shown to further enhance the catalytic activity for Suzuki-Miyaura cross-coupling reaction [20], the efficiency of organic dye removal [21], the performance of supercapacitors [22], and the sensitivity and selectivity of “turn off-on” fluorescent sensor for the detection of tertiary butylhydroquinone [23]. However, Sm-based MOFs, especially Sm/UiO-66 for chemically modified sensors, have not been exploited extensively [24]. In this study, we present the synthesis of Sm/UiO-66 and its use as a new electrode modifier for the electrochemical detection of ETB in pharmaceutical products. The structural features of Sm/UiO-66 were analyzed, and its electrocatalytic activity toward ETB oxidation was assessed. By combining the high stability of UiO-66 with the redox-active properties of Sm, the proposed Sm/UiO-66 modified electrode demonstrated increased sensitivity, selectivity, and stability.

Experimental

Materials

Zirconium chloride ($ZrCl_4$), Benzene-1,4-dicarboxylic acid (H_2BDC), samarium oxide (Sm_2O_3), N, N-dimethylformamide (DMF), methanol, and hydrochloric acid (37 %) were purchased from Sigma-Aldrich and used without further purification. Ethambutol hydrochloride (ETB) standard was obtained from a certified pharmaceutical supplier. All other reagents were of analytical grade, and deionized water was used throughout the experiments. Boric acid (H_3BO_3), phosphoric acid (H_3PO_4), acetic acid (CH_3COOH) and sodium hydroxide (NaOH) for preparing Britton-Robinson buffer (BRS) solution.

Synthesis of Sm/UiO-66

Solution 1: A mixture of 0.0530 g of $ZrCl_4$, 0.038 g of H_2BDC and 5 mL of DMF was ultrasonically dispersed. Solution 2: A mixture of 0.0198 g of Sm_2O_3 and 4.74 mL of 0.12 M HCl was ultrasonically dispersed. Then, 0.474 mL of Solution 2 was added to Solution 1, followed by a hydrothermal treatment at 120 °C for 36 h. The product obtained after hydrothermal treatment was a transparent gel, which was washed with DMF once daily for 1 day, then washed with methanol and dried at 60 °C overnight. The resulting sample was denoted as Sm/UiO-66 (5/100), where the value in parentheses refers to the initial molar ratio of Sm/Zr. Similarly, the samples UiO-66, Sm/UiO-66 (1/100), Sm/UiO-66 (3/100), Sm/UiO-66 (5/100) and Sm/UiO-66 (7/100) were synthesized by replacing the volume of Solution 2 with 0.000, 0.095, 0.284, 0.663 and 0.853 mL, respectively.

Electrode modification

A glassy carbon electrode (GCE, 3 mm diameter) was polished with alumina slurry (0.05 µm), rinsed thoroughly with distilled water, and sonicated in 1M HNO_3 and ethanol. To prepare the modified electrode, 5 mg of Sm/UiO-66 was ultrasonically dispersed in 5 ml distilled water for 8 h. A 5 µL aliquot of the suspension was dropped-cast onto the GCE surface and dried at room temperature to form Sm/UiO-66/GCE.

The used electrode was regenerated before each measurement as follows. After each measurement, the modified GCE was rinsed with distilled water and gently polished on filter paper to completely remove the modifier layer until a mirror-like surface was achieved. The electrode was then washed with 1 M HNO_3 and ethanol to clean the surface, and afterward, the cleaned electrode was modified with Sm/UiO-66 as described above.

Characterization

The structure and morphology of UiO-66 and Sm/UiO-66 were characterized by X-ray diffraction (XRD, Bruker D8 Advance), scanning electron microscopy (SEM, JEOL JSM-7610F), Electrochemical impedance spectra (EIS) were conducted on an Autolab PGSTAT302N instrument, EDX-mapping was performed using Hitachi S-4800 FESEM (Japan), and XPS was performed using an ESCA-3400 (Shimadzu) with Mg Kα radiation.

Electrochemical measurements

Electrochemical experiments were performed on a potentiostat/galvanostat CPA-HH5 electrochemical analyzer using a conventional three-electrode system with Sm/UiO-66/GCE as working electrode, Ag/AgCl (3 M KCl) as reference electrode, and platinum wire as counter electrode. All measurements were conducted in Britton-Robinson buffer solution (0.1 M BRS). Cyclic voltammetry (CV) and differential pulse voltammetry (DPV) were used to evaluate the electrochemical response toward ETB.

Electrochemical impedance spectra (EIS) were recorded using a multichannel potentiostat (VSP-3, Bio-Logic, France) over a frequency range from 10^5 to 0.01 Hz at the open-circuit potential (OCP) with an AC amplitude of 10 mV.

Real sample analysis

The applicability of the proposed sensor was assessed by measuring ETB in three tablets of ETB products and three samples of human urine. For tablets, an accurately weighed portion was ground, dissolved in water, and filtered; for human urine, an aliquot was appropriately diluted with BRS buffer. The ETB content was determined using the Sm/UiO-66/GCE sensor under optimized DPV conditions.

Results and discussion

Materials characterization

The characteristic reflections in XRD patterns of UiO-66 at $2\theta \approx$ 7.4, 8.5, 12.0, 14.0, 17.0 and 25.7° (matching the simulated UiO-66 pattern, CCDC No. 733458) are clearly visible in all samples, indicating that the framework's crystallinity remains intact after Sm incorporation (Figure 1A). As the Sm content increases (from 1/100 to 7/100), the peak intensity gradually diminishes and broadens, suggesting a decline in crystallinity due to lattice distortion and defect formation induced by Sm doping. In addition, no additional diffraction peaks corresponding to Sm_2O_3 or other crystalline impurities (JCPDS No. 15-0813) are observed, confirming the successful integration of Sm into the UiO-66 framework without forming secondary phases. EDX analysis reveals a steady increase in the Sm/Zr atomic ratio with the nominal feed, verifying successful Sm incorporation into the UiO-66 framework (Table 1). For Sm/UiO-66 synthesized with initial Sm/Zr molar ratios of 1/100, 3/100, 5/100 and 7/100, the actual Sm atomic percentages determined by EDX were 0.93, 2.25, 4.29, and 5.69 at.%, respectively (Table 1). The crystallite size (*D*), calculated from the XRD patterns using Scherrer's equation [25], decreased markedly with Sm doping, from approximately ~50 nm for pristine UiO-66 to ~ 12 nm at an initial Sm/Zr molar ratio of 3/100. This reduction suggests that Sm incorporation effectively inhibited crystal growth during hydrothermal synthesis.

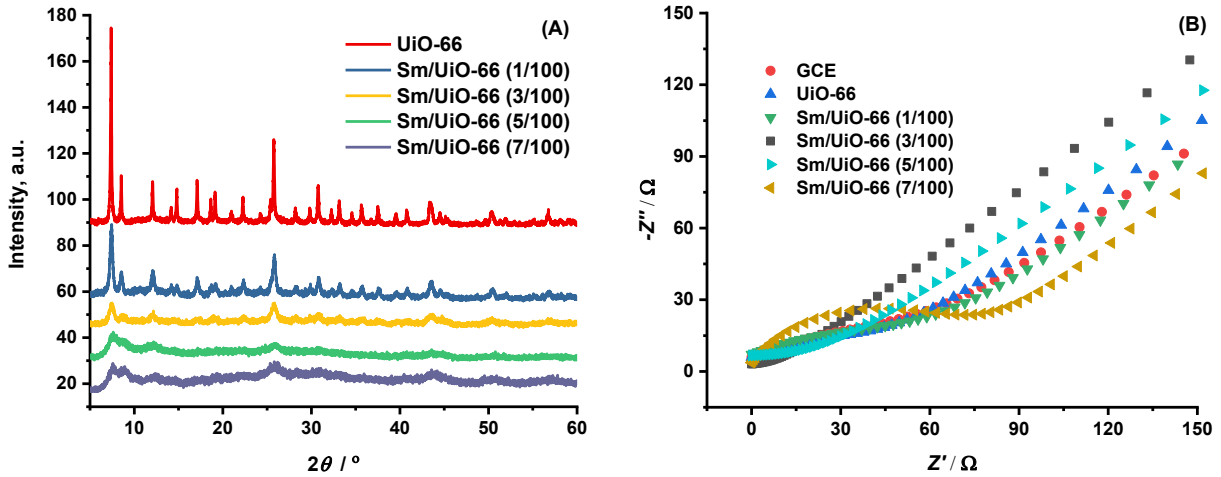

Figure 1. *A) XRD patterns of pristine UiO-66 and Sm/UiO-66 composites with various initial Sm/Zr molar ratios and B) Nyquist plots of bare GCE, UIO-66 and different Sm/UiO-66 modified electrodes, recorded in 0.1 M KCl with 10 mM $Fe(CN)_6^{3-}/Fe(CN)_6^{4-}$ with 5 mV AC amplitude*

In the Nyquist plot of electrochemical impedance spectroscopy (EIS), the semicircle at higher frequencies corresponds to the electron-transfer-limited process, and the linear portion at lower frequencies corresponds to the diffusion process. Therefore, the charge-transfer resistance (R_{ct})

represents the interfacial electron-transfer resistance at the electrode/electrolyte interface. Impedance spectra presented in Figure 1B showed a marked reduction in the R_{ct} upon Sm doping. While UiO-66 exhibited a high R_{ct} of ~60.04 Ω, this value decreased to ~30.60 Ω for Sm/UiO-66 (3/100). This substantial improvement in electron transfer can be attributed to introducing redox-active Sm species that enhance conductivity (Table 1). However, at higher doping levels (5/100 and 7/100), R_{ct} increased again, suggesting an over-doping effect that may block active sites or disrupt the framework conductivity.

Table 1. *The results of some physical chemistry characterization of Sm/UiO-66*

Notation	Molar ratio of Sm/Zr	EDX Ag/Cr molar ratio	D / nm	R_{ct} / Ω	A / cm^2
GCE	-	-	-	59.04	0.0371
UiO-66	-	-	50.3518	60.04	0.0393
Sm/UiO-66 (1/100)	0.01	0.0093	22.2242	54.73	0.0430
Sm/UiO-66 (3/100)	0.03	0.0250	11.9591	36.60	0.0559
Sm/UiO-66 (5/100)	0.05	0.0429	5.6801	40.46	0.0446
Sm/UiO-66 (7/100)	0.07	0.0569	5.8480	75.79	0.0430

Figure 2 presents CV responses of bare GCE, UiO-66 and all four Sm/UiO-66 electrodes at different scan rates, showing linear dependences of peak current values *vs*. the square root of scan rate in the insets.

Based on Figure 2, the electroactive surface area of the electrode (A) values were obtained using the Randles-Ševčik Equation (1) [26].

$$I_p = 2.68648\times10^5 n^{3/2} A D_0^{1/2} C_O v^{1/2} \quad (1)$$

where I_p / A is peak current, n is the number of electrons transferred in the redox event (usually 1), D_0 / cm^2 s^{-1} is the diffusion coefficient for the redox active species, C_O / mol cm^{-3} is the concentration of the redox active species, A / cm^2 is the electroactive surface area of the electrode and v / V s^{-1} is the scan rate.

The calculated values of A are listed in Table 1, reaching a peak value of 0.0559 cm² at the optimal Sm/Zr molar ratio of 3/100, compared to 0.0393 cm² for UiO-66 and 0.0371 cm² for bare GCE. This confirms that moderate Sm addition enhances the accessibility of electroactive sites, thereby improving electrode performance. The consistent increase in Sm content aligns well with the observed structural and electrochemical changes. Overall, these results show that the Sm/UiO-66 (3/100) composite offers the best balance among particle size reduction, charge transfer resistance, and electroactive surface area, making it the most suitable composition for further electrochemical applications.

The SEM image of pristine UiO-66 in Figure 3A, shows uniform, well-defined octahedral crystals with smooth surfaces and particle sizes around 200 to 500 nm, indicating high crystallinity. In contrast, the Sm/UiO-66 (3/100) sample in Figure 3B, displays particles with a less clear octahedral shape. The addition of Sm to the framework results in rougher surfaces, partial distortion of crystal facets, and increased particle aggregation, while the overall submicrometer size range remains unchanged. These morphological observations are consistent with the XRD results, in which UiO-66 exhibits sharp, intense diffraction peaks, while Sm/UiO-66 (3/100) shows broadened peaks and reduced intensities, indicating a slight loss of crystallinity due to lattice distortion induced by Sm doping.

The EDX-mapping of Sm/UiO-66 (3/100) in Figure 4 confirms the presence of carbon, oxygen, and zirconium as the principal elements, which is consistent with the expected composition of the UiO-66 framework.

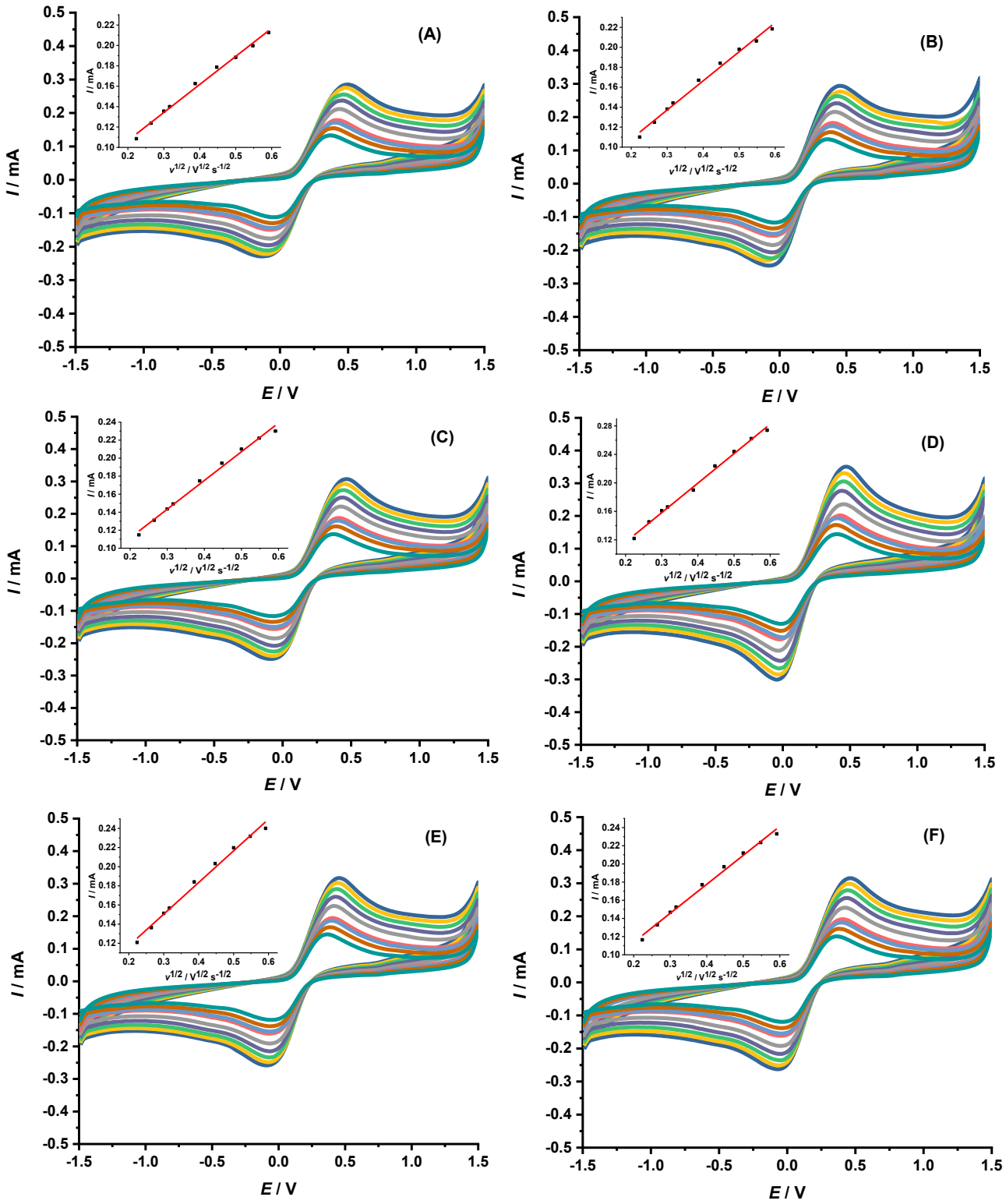

Figure 2. *Cyclic voltammetry (CV) responses at different scan rates (0.05 to 0.35 V s^{-1}) of A) bare GCE, B) UiO-66/GCE and C) Sm/UiO-66/GCE (1/100), D) Sm/UiO-66/GCE (3/100), E) Sm/UiO-66/GCE (5/100) and F) Sm/UiO-66/GCE (7/100) in 0.1 M KCl with 10 mM $[Fe(CN)_6]^{3-}$/$[Fe(CN)_6]^{4-}$. Inset curves: the linear regression between the anodic peak current and the square root of the scan rate*

Quantitative analysis shows that C and O account for 61.11 and 34.86 at.%, respectively, while Zr and Sm contribute 3.93 and 0.10 at.%, respectively. The mapping demonstrates that C and O are homogeneously dispersed throughout the framework.

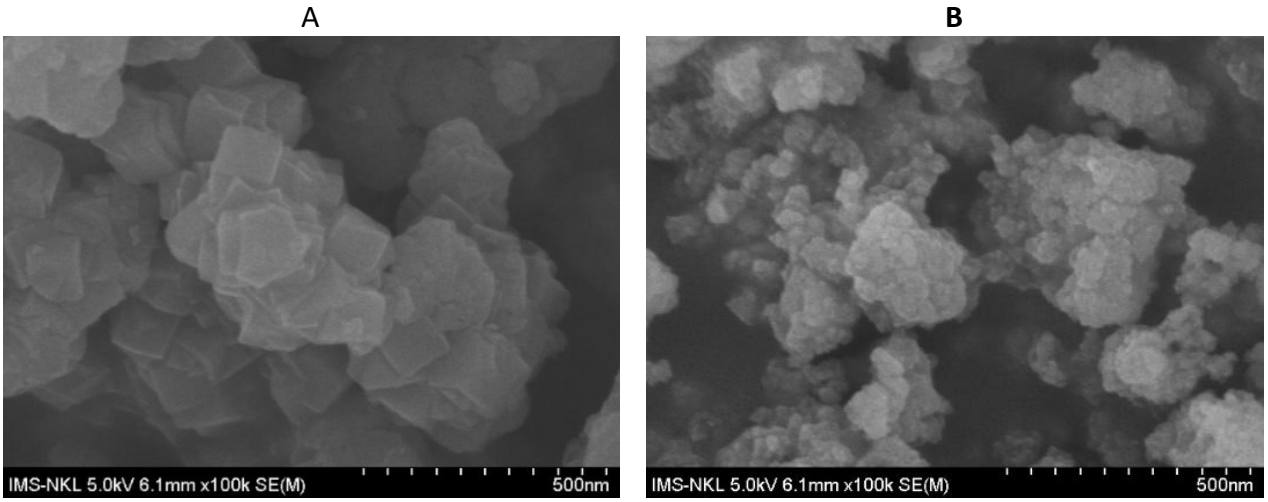

Figure 3. *SEM images of A) pristine UiO-66 and B) Sm/UiO-66 (3/100)*

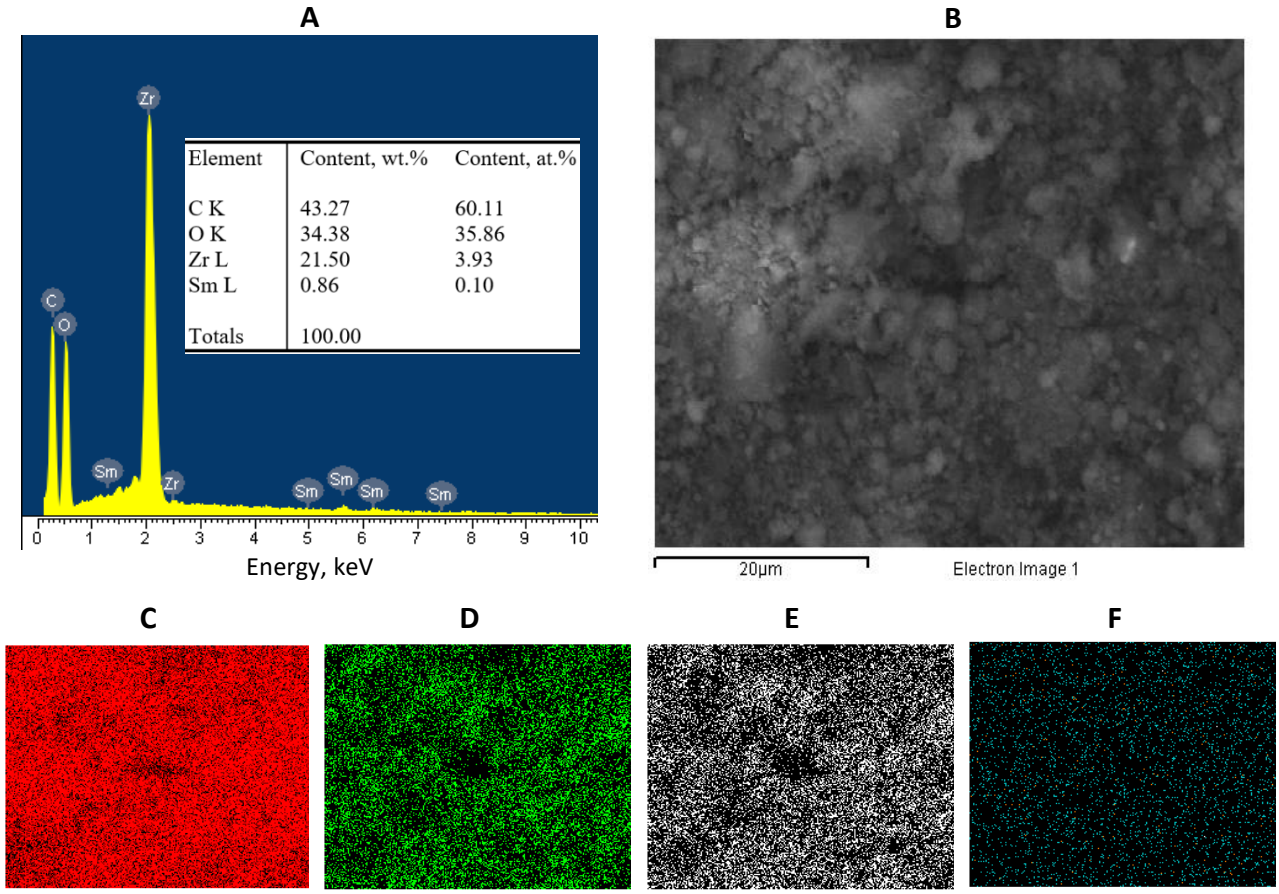

Figure 4. *A) EDX spectrum, B) electron image of Sm/UiO-66 and EDX mapping of C) Zr, D) O, E) C and F) Sm*

Notably, the Sm signal is uniformly distributed and co-localized with Zr, suggesting that Sm species are well-dispersed and anchored within the framework rather than forming separate clusters or aggregates. This homogeneous distribution of Sm strongly supports the hypothesis that samarium is successfully incorporated into the UiO-66 structure in a dispersed form, thereby potentially generating additional active sites while maintaining the integrity of the parent framework.

The surface chemical composition and oxidation states of the Sm/UiO-66 composite were investigated by XPS as shown in Figure 5. The survey spectrum confirms the presence of Sm, Zr, O and C, indicating the successful incorporation of samarium species into the UiO-66 framework without

introducing additional impurities (Figure 5A). The high-resolution Sm 3d spectrum exhibits two characteristic peaks located at binding energies of approximately 1085.9 eV and 1112.3 eV, which are assigned to the Sm $3d_5/_2$ and Sm $3d_3/_2$ components, respectively (Figure 5B).

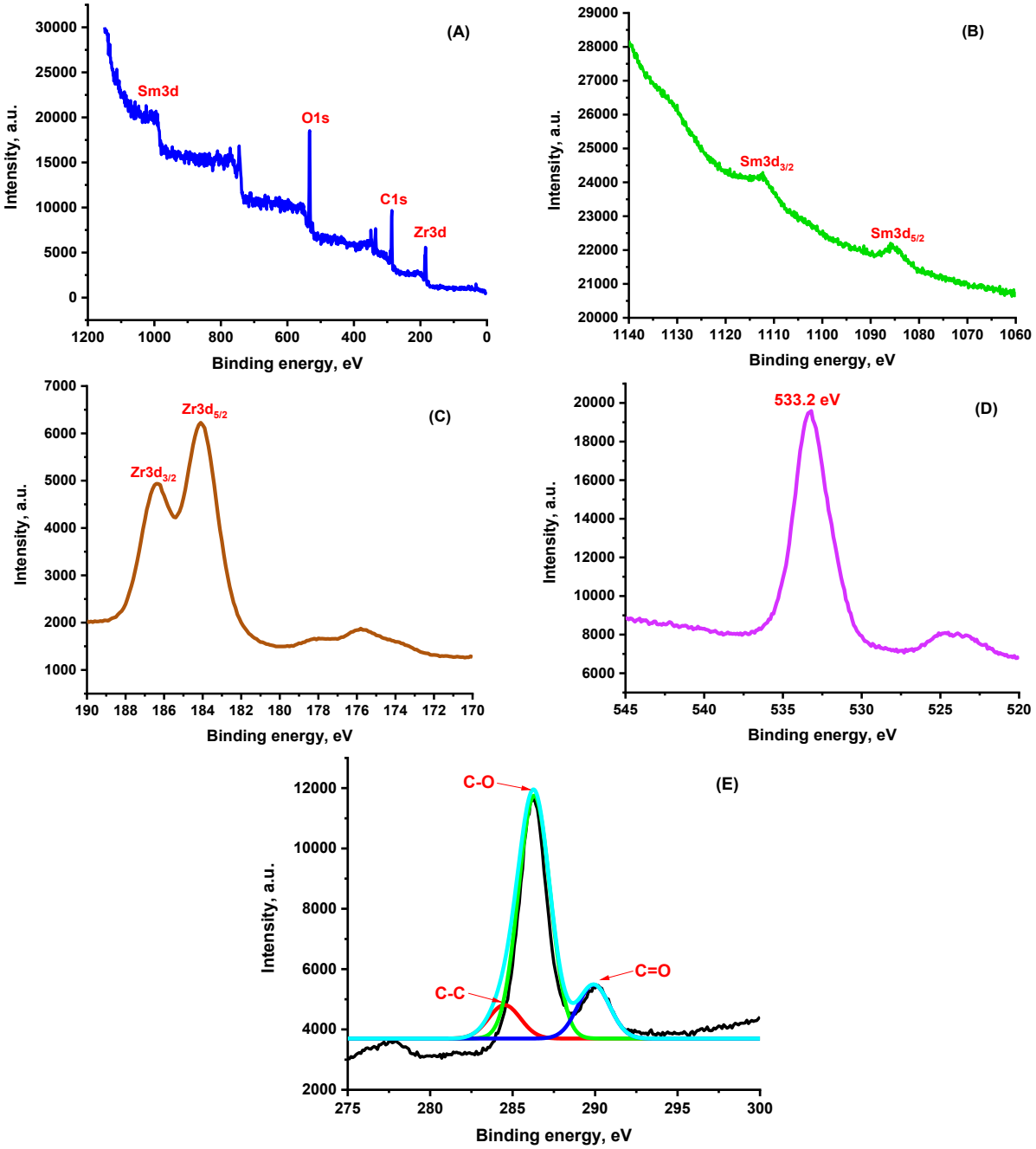

Figure 5. *XPS spectra of Sm/UiO-66: (A) survey spectrum; (B) high-resolution Sm 3d spectrum; (C) high-resolution Zr 3d spectrum; (D) high-resolution O 1s spectrum; and (E) high-resolution C 1s spectrum*

These binding energy values are consistent with those reported for Sm^{3+} species, suggesting that samarium is present predominantly in the trivalent oxidation state [27]. The Zr 3d spectrum (Figure 5C) shows two well-defined peaks at~182.4 eV (Zr $3d_5/_2$) and ~184.1 eV (Zr $3d_3/_2$), which are characteristic of Zr^{4+} in the Zr–O clusters of UiO-66 [28]. The preservation of these binding energies after Sm modification demonstrates that the zirconium oxo-clusters remain structurally intact and that the introduction of Sm does not disrupt the original UiO-66 framework. The O 1s spectrum (Figure 5D) displays a dominant peak centered at ~533.2 eV, which can be attributed mainly to Zr–O and Sm–O bonds, along with contributions from C=O and C–O groups of the terephthalate linkers [28].

The fitting peaks of C 1s at 284.6, 286.1 and 288.7 eV (Figure 5E) assign to C-C, C-O, and C=O bonds related to the terephthalate structure in UiO-66(Zr)-2OH [28]. These features are typical for UiO-66-based materials and confirm that the organic framework is preserved after Sm incorporation.

Collectively, the XPS results confirm the successful synthesis of Sm/UiO-66, with samarium existing predominantly as Sm^{3+} and zirconium retaining its Zr^{4+} oxidation state. The coexistence of Sm–O and Zr–O bonding environments, along with intact organic linker signals, indicates that Sm species are introduced effectively without destroying the UiO-66 framework. This stable chemical environment is expected to contribute positively to the enhanced catalytic/electrochemical performance of Sm/UiO-66 in subsequent applications.

Electrochemical determination of ETB using Sm/UiO-66/GCE

The electrocatalytic behavior of Sm/UiO-66 composites toward ETB oxidation was examined by varying the samarium (Sm) content from 1/100 to 7/100 relative to pristine UiO-66 and bare GCE. As shown in Figure 6A, the bare GCE exhibits a negligible current response, whereas UiO-66/GCE shows only a modest enhancement of anodic current due to its limited conductivity. Incorporation of Sm into the UiO-66 framework markedly improved the anodic current response, reflecting enhanced charge transport and the introduction of new catalytic sites. Among the electrodes with different ratios, Sm/UiO-66 (3/100) exhibited the highest anodic peak current (Figure 6B). This optimal performance suggests that a moderate level of Sm incorporation provides a synergistic effect: the MOF framework provides high surface area and adsorption capacity for ETB molecules, while the redox-active Sm centers (Sm^{3+}/Sm^{2+}) facilitate electron shuttling during oxidation. The electron-transfer mediation by Sm ions accelerates the kinetics of ETB electro-oxidation, leading to a pronounced current response.

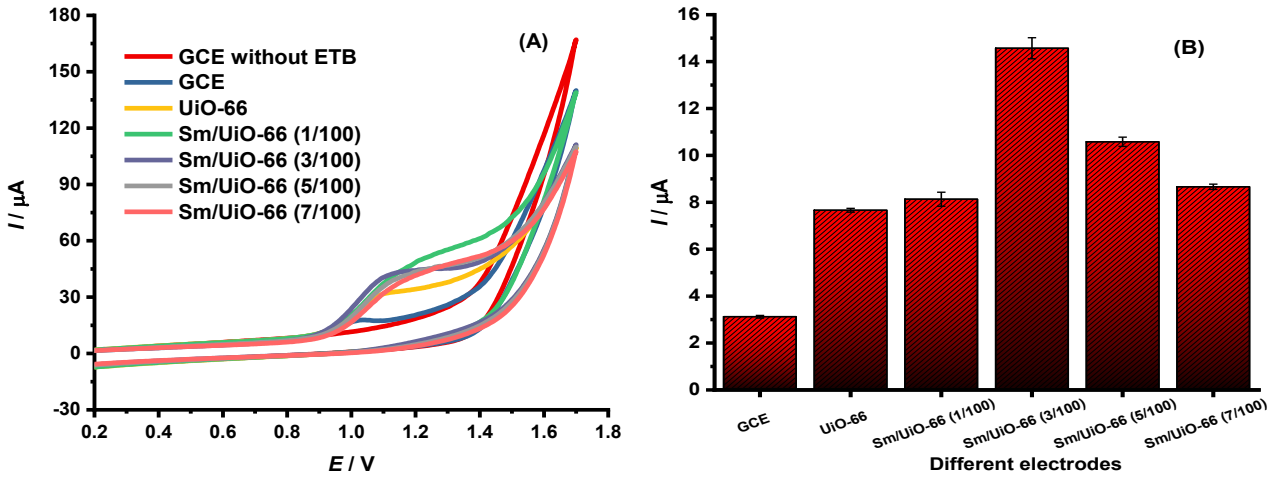

Figure 6. *(A) CV curves of different electrodes with C_{ETB} = 25.0 µM in 0.1 M BRS buffer (pH 6), potential scan rate v = 0.2 V s^{-1}; (B) anodic peak current intensities at different electrodes (3 replicate measurements)*

The current response gradually declined at higher Sm loadings (≥ 5/100). This possibility may arise from the aggregation of excess Sm species, partial pore blockage that hinders ETB diffusion into the UiO-66 structure, and disruption of framework crystallinity, which collectively reduce the effective electroactive surface area. This attenuation agrees with the decrease in electroactive surface area and increase in electron transfer resistance due to overloading Sm, as discussed above.

pH effect on EBT response at Sm/UiO-66(3/100)/GCE

The electrochemical response of Sm/UiO-66(3/100)/GCE toward ETB is strongly influenced by solution pH, with the anodic current peaks shifting to more negative potentials as pH increases. (Figure 7A). As shown in Figure 7B, the current response at pH 3 is weak (~3 µA), but it increases

sharply with rising pH, reaching a maximum at pH 4 (~16.8 µA). Between pH 5 and 7, the current intensity remains relatively high (14 to 14.6 µA), indicating that the electrode maintains stable electrocatalytic activity in this moderately acidic to near-neutral region. At alkaline conditions (pH 8), the signal declines significantly (~4.3 µA), suggesting that proton deficiency hinders ETB oxidation. Along with current variations, the oxidation peak potential shifts negatively as pH increases in a linear manner (Figure 7C).

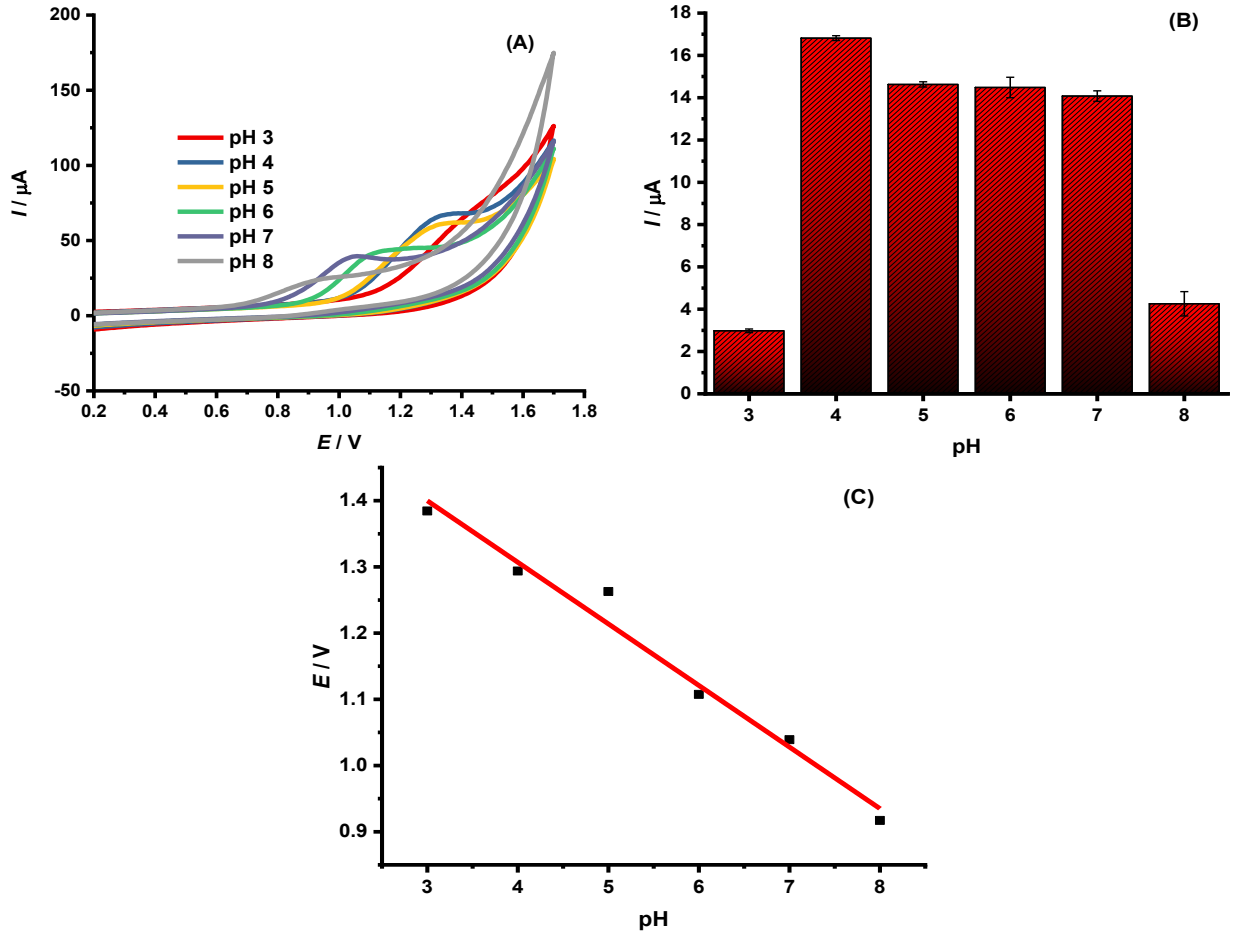

Figure 7. *(A) CV curves of Sm/UiO-66 (3/100)/GCE recorded in 0.1 M BRS buffer at different pH values (3 to 8) containing C_{ETB} = 25.0 µM with a scan rate of 0.2 V s^{-1}, (B) dependence of the anodic peak current intensity on pH and (C) linear dependence (with the best-fit line) of the anodic peak potential (E_p) vs. pH*

The linear regression equation (Equation (2)) obtained from the E_p- pH plot is:

E_{ETB} = (1.679 ± 0.040) + (-0.093 ± 0.007) pH, r^2 = 0.978 (2)

The slope of approximately -0.093 mV pH^{-1} is larger than the theoretical Nernstian value (-0.059 mV pH^{-1}), indicating that protons are involved in the rate-determining step. However, the process may involve multiple or two protons per electron and/or be influenced by adsorption effects and quasi-reversible electron transfer. The good linearity (r^2 ≈ 0.98) confirms the strong pH dependence of the redox mechanism. Overall, these results demonstrate that pH 4 provides the most favorable conditions, combining the highest current response with a predictable potential shift, and was selected as the optimal pH for further analytical studies of ETB at Sm/UiO-66 (3/100)/GCE.

The oxidation peak current of ETB at Sm/UiO-66(3/100)/GCE increases as the scan rate increases from v = 0.03 to 0.30 V s^{-1} (Figure 8A). A linear I_p - $v^{1/2}$ relationship (Figure 8B) is defined as: I_{ETB} = (1.854 ± 0.503) + (32.320 ± 1.356) $v^{1/2}$, r^2 = 0.988. It is clear that the intercept of this line does

not pass the origin, demonstrating that the oxidation process is adsorption-controlled [29]. Concomitantly, the peak potential shifts positively with increasing scans, and E_p - ln v dependence is highly linear (Figure 8C): E_{ETB} =(1.1975 ± 0.0057) + (0.0415 ± 0.0024) ln v, r^2 = 0.996, indicating quasi-reversible charge transfer [30]. From Laviron's relation for an anodic process slope = $RT/(\alpha nF)$ [31], the slope approximately 0.0415 V gives αn ≈ 0.62. Assuming a typical $\alpha \approx 0.5$ for an irreversible system [32], n is ≈ 1.2 ≈ 1 electron. When combined with the pH-dependence, which implies the number of protons is 1. Therefore, the overall stoichiometry is consistent with one proton-electron oxidation. The available data related to the oxidation mechanism of ETB are limited, and some studies suggest that the reaction involves two electrons and one proton [33]. The observed differences may be attributed to the different nature of the electrode modification materials.

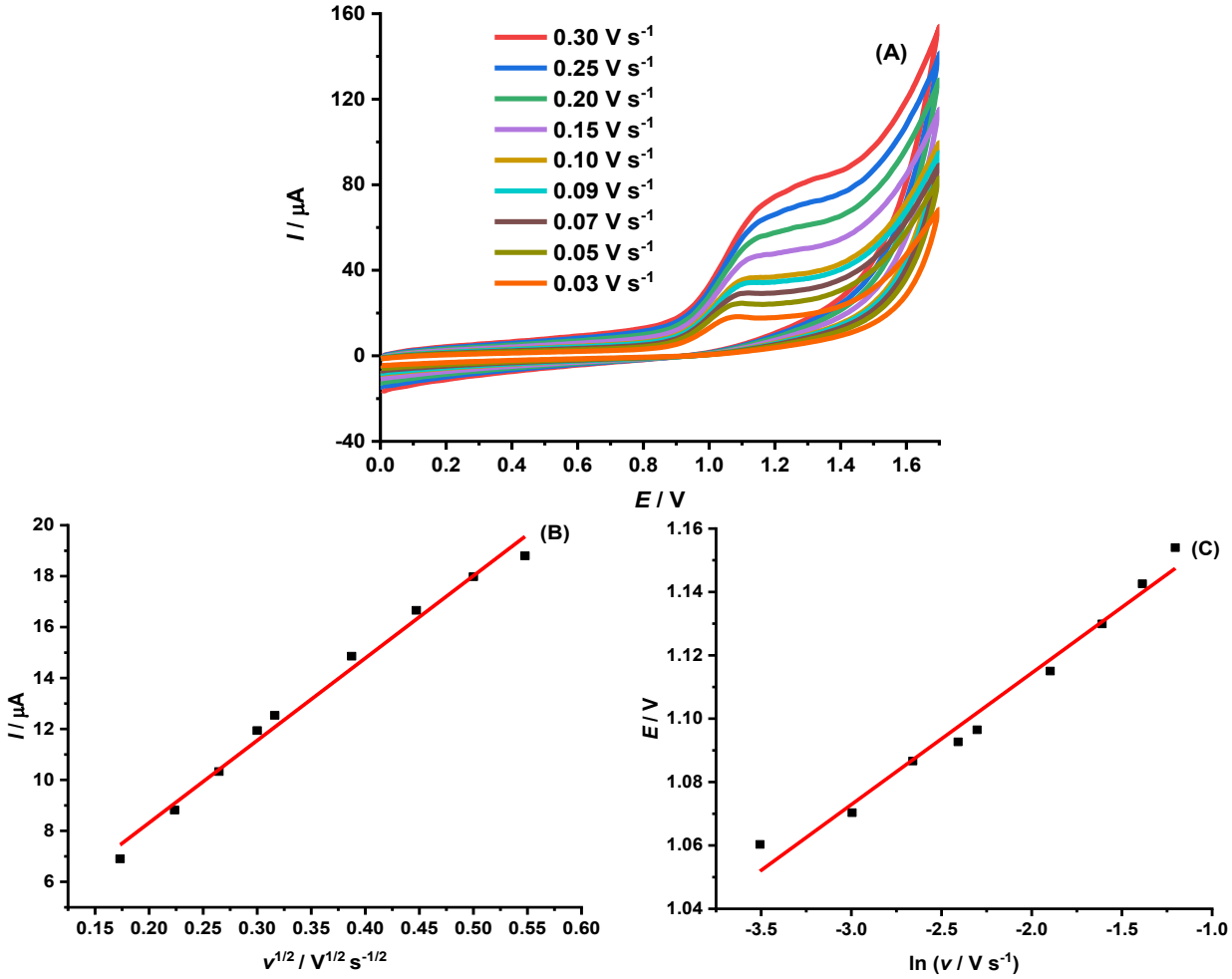

Figure 8. *(A) CVs of Sm/UiO-66(3/100)/GCE in 0.1 M BRS buffer (pH 4) containing* C_{ETB} *= 25.0 µM recorded at different scan rates, (B) linear relationship between* I_p *and* $v^{1/2}$*) and (C) dependence of* E_p *on ln* v

Optimizing the operational parameters of DPV method

In this study, DPV parameters, *i.e*. accumulation time, potential time, pulse amplitude, and voltage step, were studied. It was found that the accumulation time, potential time, pulse amplitude, and voltage step of 0, 4, 0.10 and 0.008 V, respectively, are suitable for peak current to achieve the highest and most stable results (Figures S1-S4, Supplementary material).

Linear range and limit of detection

To create the calibration curve, the supporting electrolyte (buffer solution) was first added to the electrochemical cell. Then, successive aliquots of the ETB standard solution (1 mM) were added, and

DPV measurements were recorded after each addition (Figure 9A). A linear regression was performed between the peak current responses and the corresponding ETB concentrations to identify the linear range(s). The oxidation peak current values of ETB at the Sm/UiO-66-modified electrode exhibit two distinct linear dynamic ranges, as confirmed by the calibration plots shown in Figure 9B. In the low concentration range of 0.5 to 9.9 µM, the peak current increases linearly with concentration following the regression equation: I_{ETB} = (1.3480±0.0228)+(0.6186±0.0043)C_{ETB}; r^2 = 0.9994 with a calculated LOD of 0.23 µM and LOQ of 0.76 µM. At higher concentrations (9.9 to 31.5 µM), the slope decreases, and the calibration equation becomes: I_{ETB} = (4.5680±0.0289)+(0.2897±±0.0014)C_{ETB}; r^2 = 0.9997, suggesting that the active sites gradually approach saturation and the sensitivity diminishes compared to the lower concentration range.

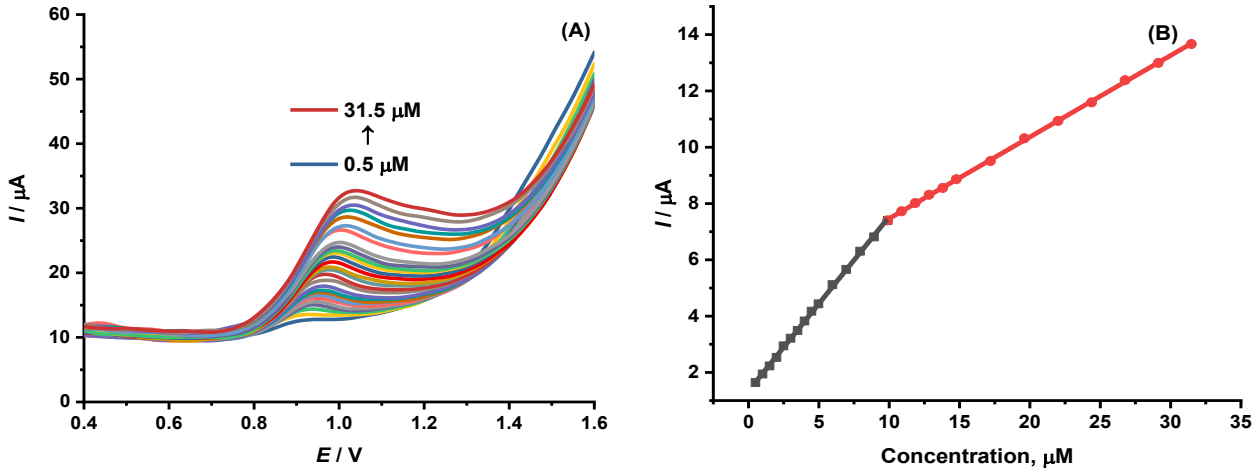

Figure 9. *(A) DPV curves of Sm/UiO-66 (3/100)/GCE recorded in 0.1 M BRS buffer solution (pH 4.0) with increasing ETB concentrations (0.5 to 31.5 µM), (B) corresponding calibration plot showing two linear relationships between peak current and ETB concentration*

Overall, the electrode provides an excellent linear response in a wide concentration range (0.5 to 31.5 µM), with high determination coefficients (r^2 > 0.999). The dual-slope behavior reflects both the high affinity of ETB towards the Sm/UiO-66 surface at low levels and the saturation effect at higher concentrations.

To further evaluate the analytical performance of the proposed Sm/UiO-66/GCE electrode, its linear range and LOD values were compared with those of other reported sensors for ETB determination (Table 2). The results show that composite-modified electrodes, such as graphite-polyurethane and graphite-paraffin electrodes, exhibited relatively high detection limits (63.4 to 100 µM) and narrower linear ranges limited to the millimolar region, making them unsuitable for trace-level analysis [34,35]. Similarly, modified electrodes based on Au-MEA and Au/PANSA/PVP-AgNPs demonstrated improved sensitivity, with LODs as low as 0.155 to 0.7 µM, but still required relatively higher ETB concentrations (2 to 2000 µM) to produce linear responses [36,37]. In contrast, the Sm/UiO-66/GCE developed in this study achieved a remarkably low LOD of 0.23 µM with two distinct linear ranges (0.5 to 9.9 and 9.9 to 31.5 µM). This performance is comparable or better than the best values reported in literature. Notably, the electrode provided reliable responses in pharmaceutical formulations and human urine samples, demonstrating its practical applicability in real matrices. Therefore, combining Sm doping with UiO-66 framework integration significantly improved the electrochemical properties of the GCE, offering both high sensitivity and broad applicability. These results confirm that the developed electrode not only provides high sensitivity and a low detection limit but also ensures robust repeatability and precision, satisfying stringent analytical performance requirements.

Table 2. *Comparison of the analytical performance of the present method with previously reported ETB sensors*

Electrode	Method	Linear range, µM	LOD, µM	Sample matrix	Ref.
Au-MEA	Amperometric	50 to 2000	0.16	Aqueous medium	[36]
P_{mel}-Au_{nano}/GCE	DPV	0.5 to 150	0.21	Human urine sample	[38]
Au/PANSA/PVP-AgNPs	Chronoamperometric	2 to 12	0.70	Serum samples	[37]
Graphite polyurethane composite electrode	Amperometric	500 to 1100	63.40	Synthetic urine	[35]
Graphite-paraffin composite electrode	Amperometric	250 to 1500	100.00	Pharmaceutical formulations	[34]
Nafion/MWCNT-SPCE	SWV	1.37×10^5 to 1.37×10^6	4000	Human urine and blood serum samples	[39]
Sm/UiO-66/GCE	DPV	0.5 to 9.9	0.23	Pharmaceutical formulations and human urines	This study

MEA: microelectrode array; P_{mel}: poly-melamine; PANSA: poly(8-anilino-1-naphtalene sulphonic acid); PVP: polyvinylpyrrolidone; nano and NPs: nanoparticles; MWCNT: multiwalled carbon nanotubes; SCPE: screen printed carbon electrode

Repeatability, reproducibility, long-term stability and interfering studies

The repeatability of the proposed method was evaluated by measuring four different ETB concentrations (2.5, 5.0, 10.0, 20.0 and 30.0 µM) (Figure S5, Supplementary material), each tested with ten replicate DPV measurements. The calculated RSD values were then compared with ½ RSD of Horwitz (RSD_H) function to assess analytical precision. As shown in Figure 10A, at all tested concentrations of ETB, the RSD values obtained for Sm/UiO-66/GCE were consistently lower than ½ RSD_H. For instance, at 2.5 µM ETB, the calculated RSD was 3.3 %, which is significantly below the ½ RSD_H of ~8.5 %. At higher concentrations, such as 19.6 and 29.1 µM, the RSD values dropped further to below 1.5 %, demonstrating good repeatability.

The reproducibility of fabricating the modified electrode was assessed using a single glassy carbon electrode. After each measurement, the electrode surface was thoroughly rinsed with distilled water, mechanically polished to fully remove the modified layer, and then re-modified using the same preparation procedure. Differential pulse voltammetry (DPV) measurements were carried out after each independent modification. This modification-measurement cycle was repeated seven times under identical conditions. The relative standard deviation (RSD) of the peak current responses was calculated to evaluate the reproducibility of the electrode fabrication process. As shown in Figure 10B, the peak current responses remained highly consistent with only minor variation, yielding a relative standard deviation (RSD) of less than 3.5 %. This demonstrates excellent reproducibility of the fabricated electrode. The long-term stability of the electrode was further investigated over a period of seven consecutive days (Figure 10C). The current response showed only a slight decrease, retaining over 95 % of its initial signal after one week of storage under ambient conditions. These results confirm that the Sm/UiO-66/GCE possesses long-term stability, which is critical for practical applications in pharmaceutical and biological analysis.

The interfering effects of some inorganic and organic substances on ETB peak currents are also shown in Figure 10 D. $MgCl_2$ (labeled as C1), KNO_3 (C2), $ZnCl_2$ (C3), NaCl (C4), $Al_2(SO_4)_3$ (C5), $(NH_4)_2SO_4$ (C6), D-Glucose (C7), ascorbic acid (C8), L-cysteine (C9), sodium benzoate (C10), urea (C11), and D-glutamic acid (C12) are used in this study. The C/C_{ETB} value in Figure 10 D was defined as the molar ratio of interferent concentration to that of ETB, in which the relative error was still less than 5 %. As shown in Figure 10D, the relative error caused by different interferents remained within ±5 %, even when their concentrations were 120 to 150 times higher than that of ETB.

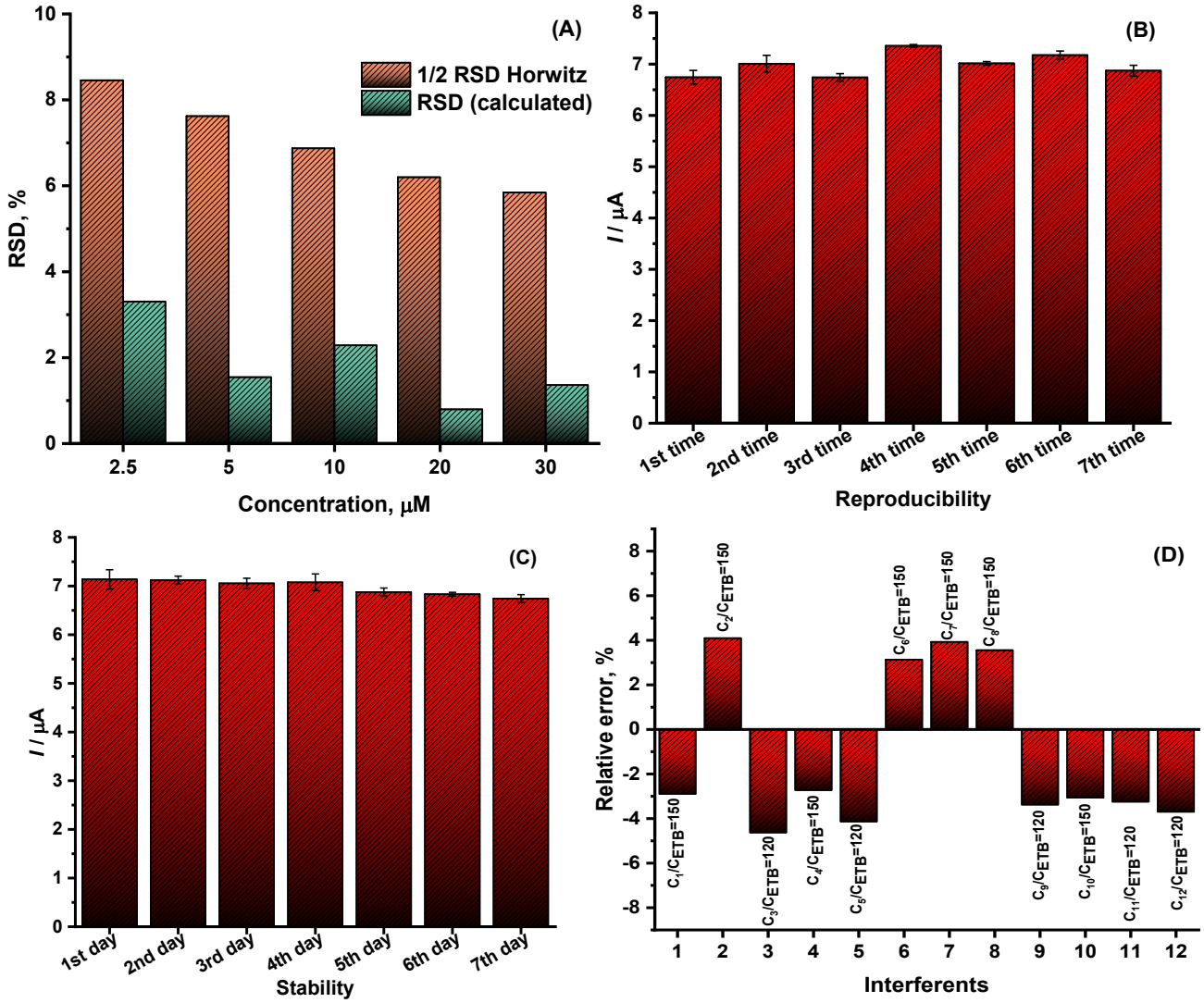

Figure 10. *(A) Comparison of RSD values with ½ RSD_H; (B) reproducibility tested by seven consecutive measurements of peak current of ETB (10.0 μM), (C) stability tested by 7-day-long term durability and (D) relative error of the influence of some interfering substances at different C/C_{ETB} ratios (C_{ETB} = 10 μM))*

This confirms that the proposed Sm/UiO-66/GCE sensor exhibits excellent selectivity toward ETB in the presence of common coexisting ions and biomolecules. The minimal influence of these interferents can be attributed to the high affinity of ETB molecules for the active sites of Sm/UiO-66 and the effective charge-transfer properties of the modified electrode. These findings demonstrate that the developed method is highly selective and reliable for measuring ETB in complex samples, such as pharmaceutical formulations and biological fluids.

Real sample analysis

The practical applicability of the proposed Sm/UiO-66/GCE sensor was confirmed by measuring ETB concentrations in three pharmaceutical formulations and three human urine samples. To further assess accuracy, spiking experiments were conducted, and the recovery values were calculated. The results (Table 3) showed excellent recoveries ranging from 95.2 to 103.8 %, demonstrating that the developed method can reliably quantify ETB in real samples without significant matrix interference.

Table 3. *The results of analyzing ETB in the pharmaceutical formulation and human urine*

Notation	ETB content* ± SD, mg	Content, µg		Recovery, %
		Spiked	Found ± SD	
Tablet 1 (Label 400 mg ETB/unit)	386.8 ± 5.3	2.7723	2.6822 ± 0.0281	96.8
Tablet 2 (Label 400 mg ETB/unit)	410.6 ± 5.1		2.8575 ± 0.0393	103.1
Tablet 3 (Label 400 mg ETB/unit)	384.0 ± 7.3		2.6404 ± 0.0295	95.2
Urine 1	N/A	5.8398	5.7569 ± 0.0754	103.8
Urine 2	N/A		5.3489 ± 0.0833	96.5
Urine 3	N/A		5.6600 ± 0.0502	102.1

*ETB content (ETB/tablet) determined by DPV; SD: standard deviation (n =3)

Conclusion

In this study, Sm-doped UiO-66 (Sm/UiO-66) was successfully synthesized and used to modify a glassy carbon electrode (GCE) for electrochemical detection of ethambutol (ETB). Structural and electrochemical analyses showed that incorporating Sm into the UiO-66 framework caused a slight decrease in intrinsic conductivity but significantly increased the effective electrochemical surface area. This enhancement improved electron-transfer kinetics and catalytic activity toward ETB. The Sm/UiO-66/GCE electrode demonstrated excellent analytical performance, including a low detection limit, along with high repeatability and stability. Additionally, interference tests confirmed the sensor's selectivity, and measurements in pharmaceutical formulations and human urine yielded recovery rates between 95.2 and 103.8 %. A statistical comparison using the *t*-test showed no significant difference from the standard HPLC method at the 95 % confidence level. These findings suggest that the Sm/UiO-66/GCE electrode is a promising, reliable, and cost-effective platform for sensitive and selective ETB detection in routine pharmaceutical analysis.

Supplementary material

Additional data are available at https://pub.iapchem.org/ojs/index.php/JESE/article/view/3213, or from the corresponding author on request.

Acknowledgement: *This research was funded partially by Hue University under the Core Research Program No NCTB.DHH.2025.05.*

Conflict of interest: *All authors declare that they have no competing interests.*

Data availability: *The datasets generated during and/or analysed during the current study are available from the corresponding author on request.*

References

[1] D. Goletti, S. Al-Abri, G.B. Migliori, C. L. Arlehamn, P. Haldar, C. Sundling, C. da Costa, K. W. To, A. R. Martineau, E. Petersen, A. Zumla, S. Shan Lee, World Tuberculosis Day 2024 theme "Yes! We can end TB"; can be made a reality through concerted global efforts that advance detection, diagnosis, and treatment of tuberculosis infection and disease, *International Journal of Infectious Diseases* **141** (2024) 106993. https://doi.org/10.1016/j.ijid.2024.106993

[2] N. Bonginkosi, D. Paolo, M. Helen, S. Peter, M. Thuli, R. Roxana, O. Philip, R.-G.J. Eduardo, Pharmacokinetics of ethambutol and weight banded dosing in South African adults newly diagnosed with tuberculosis and HIV, *Antimicrobial Agents and Chemotherapy* **69** (2025) e01200-24. https://doi.org/10.1128/aac.01200-24

[3] P. Garg, R. Garg, R. Prasad, A. K. Mishra, A prospective study of ocular toxicity in patients receiving ethambutol as a part of directly observed treatment strategy therapy, *Lung India* **32** (2015) 16-19. https://doi.org/10.4103/0970-2113.148428

[4] P. Kulniwatcharoen, L. Hansapinyo, N. Chattipakorn, S.C. Chattipakorn, Potential underlying mechanisms of ethambutol induced optic neuropathy: Evidence from in vitro to clinical studies, *Food and Chemical Toxicology* **182** (2023) 114176. https://doi.org/10.1016/j.fct.2023.114176
[5] R. Mereškevičienė, E. Danila, The adverse effects of tuberculosis treatment: a comprehensive literature review, *Medicina (Buenos Aires)* **61** (2025) 911. https://doi.org/10.3390/medicina61050911
[6] H. Ruan, Y. Luo, Q. Yang, C. Liu, Y. Shi, M. Ye, L. Hong, W. Su, A novel derivatization-free approach for analysis of (+)2-aminobutanol and ethambutol hydrochloride in tablets preparation using RP-HPLC-NQAD, *Biomedical Chromatography* **39** (2025) e70049. https://doi.org/10.1002/bmc.70049
[7] W.-Y. Wu, J.-Y. Yang, L.-M. Du, H. Wu, C.-F. Li, Determination of ethambutol by a sensitive fluorescent probe, *Spectrochimica Acta A* **79** (2011) 418-422. https://doi.org/10.1016/j.saa.2011.02.045
[8] F. Han, W. Li, Y. Jin, F. Wang, B. Yuan, H. Xu, Rapid and sensitive LC-MS/MS method for simultaneous determination of three first-line oral antituberculosis drug in plasma, *Journal of Chromatographic Science* **59** (2021) 432-438. https://doi.org/10.1093/chromsci/bmaa130S
[9] R. F. Ajayl, S. Tshoko, Y. Mgwili, S. Nqunqa, T. Mulaudzi, N. Mayedwa, E. Iwuoha, Green method synthesised graphene-silver electrochemical nanobiosensors for ethambutol and pyrazinamide, *Processes* **8** (2020) 879. https://doi.org/10.3390/pr8070879
[10] R. R. F. Fonseca, R. de Q. Ferreira, P. P. Luz, MOF-modified electrodes applied as electrochemical sensors for voltammetric determinations, *Journal of Solid State Electrochemistry* **29** (2025) 837-854. https://doi.org/10.1007/s10008-024-05985-5
[11] N.A.A. Salman, I.A. Jassem, I.N. Taeb. A simple UiO-66-NH_2@MWCNTs based electrochemical sensor for the sensitive detection of metronidazole: Original scientific article, *ADMET and DMPK* **13** (2025) 2940. https://doi.org/10.5599/admet.2940.
[12] Y. Ding, F. Wei, C. Dong, J. Li, C. Zhang, X. Han. UiO-66 based electrochemical sensor for simultaneous detection of Cd(II) and Pb(II), *Inorganic Chemistry Communications* **131** (2021) 108785. https://doi.org/10.1016/j.inoche.2021.108785.
[13] Y. Liao, J. Tang, Z. He, X. Cheng, Z. Wang, L. Tang, A portable electrochemical device with UiO-66@polydopamine modified screen-printed electrodes for rapid detection of manganese ions, *Microchimica Acta* **192** (2025) 612. https://doi.org/10.1007/s00604-025-07459-5
[14] M. Chandran, B. Dhanasekaran, M. Veerapandian, S. Govindaraju, K. Yun, Porous polymer-modified metal-organic framework (AM@UIO-66-NH_2) for electrochemical detection of dopamine in human serum, *Microporous and Mesoporous Materials* **396** (2025) 113726. https://doi.org/10.1016/j.micromeso.2025.113726
[15] A.M. Pourrahimi, S. Tajik, F. Garkani Nejad, H. Beitollahi, Simultaneous voltammetric determination of morphine and tramadol using zirconium-based metal organic framework modified electrode, *Topics in Catalysis* **68** (2025) 551-561. https://doi.org/10.1007/s11244-024-01999-5
[16] C. R. Michel, A. H. Martínez-Preciado, R. Parra, C. M. Aldao, M. A. Ponce, Novel CO_2 and CO gas sensor based on nanostructured Sm_2O_3 hollow microspheres, *Sensors and Actuators B: Chemical* **202** (2014) 1220-1228. https://doi.org/10.1016/j.snb.2014.06.038
[17] E. A. Boyd, C. Shin, D. J. Charboneau, J. C. Peters, S. E. Reisman, Reductive samarium (electro)catalysis enabled by SmIII-alkoxide protonolysis, *Science* **385** (2024) 847-853. https://doi.org/10.1126/science.adp5777

[18] R. Chen, Y. Bai, B. Wei, Samarium redox catalysis, *Chemical Synthesis* **5** (2025) 62. https://doi.org/10.20517/cs.2025.22
[19] K. Zhang, T. H. Lee, M.-J. Choi, A. Rajabi-Abhari, S. Choi, K. S. Choi, R. S. Varma, J.-W. Choi, H. W. Jang, M. Shokouhimehr, Electrochemical activity of Samarium on starch-derived porous carbon: rechargeable Li- and Al-ion batteries, *Nano Convergence* **7** (2020) 11. https://doi.org/10.1186/s40580-020-00221-y
[20] L.-X. You, Y. Xu, F. Zhang, J.-H. Hao, S.-Y. Xie, G. Xiong, A.S. Potapov, F. Ding, Y.-G. Sun, A novel N-heterocyclic carbene-palladium modified metal-organic framework (Sm-MOF-Pd) for Suzuki-Miyaura cross-coupling reaction, *Polyhedron* **242** (2023) 116493. https://doi.org/10.1016/j.poly.2023.116493
[21] G. Yang, D. Zhang, G. Zhu, T. Zhou, M. Song, L. Qu, K. Xiong, H. Li, A Sm-MOF/GO nanocomposite membrane for efficient organic dye removal from wastewater, *RSC Advances* **10** (2020) 8540-8547. https://doi.org/10.1039/D0RA01110J
[22] S. Rajasekaran, S. D. K R, B. S. Reghunath, B. Saravanakumar, J. J. William, D. Pinheiro, Sm-MOF/rGO/PANI composite as an electrode material for supercapacitor applications, *Electrochimica Acta* **467** (2023) 143031. https://doi.org/10.1016/j.electacta.2023.143031
[23] X. Liu, X. Zhang, R. Li, L. Du, X. Feng, Y. Ding, A highly sensitive and selective “turn off-on” fluorescent sensor based on Sm-MOF for the detection of tertiary butylhydroquinone, *Dyes and Pigments* **178** (2020) 108347. https://doi.org/10.1016/j.dyepig.2020.108347
[24] S. Biswas, Q. Lan, C. Li, X.-H. Xia, Morphologically flex Sm-MOF based electrochemical immunosensor for ultrasensitive detection of a colon cancer biomarker, *Analytical Chemistry* **94** (2022) 3013-3019. https://doi.org/10.1021/acs.analchem.1c05538
[25] A. L. Patterson, The Scherrer formula for X-Ray particle size determination, *Physical Review* **56** (1939) 978-982. https://doi.org/10.1103/PhysRev.56.978
[26] V. Jangra, H. Kaur, N. Kumar, U. Kumar, P. K. Sonkar, L. B. Prasad, Electrochemical determination of antipsychotic drug quetiapine fumarate using hexagonal nickel oxide nanoparticle decorated functionalized multiwalled carbon nanotubes, *Electrochimica Acta* **531** (2025) 146432. https://doi.org/10.1016/j.electacta.2025.146432
[27] J. Meng, J. Teng, F. Li, T. Li, R. Greco, W. Cao, Sm-MOF decorated cotton for efficient on-demand oil-water separation and organic pollutants removal, *Separation and Purification Technology* **358** (2025) 130248. https://doi.org/10.1016/j.seppur.2024.130248
[28] Y. Gao, Q. Chen, X. Shen, S. Yao, Z. Jiang, S. Ma, H. Yang, J. Li, Z. Lin, X. Liu, UiO-66(Zr)-$_2$OH-supported Pd0 NP catalysts accelerated a Fenton-like reaction: Iron cycling and hydrogen peroxide generation achieved simultaneously, *ACS Applied Materials & Interfaces* **16** (2024) 62171-62184. https://doi.org/10.1021/acsami.4c13995
[29] J. Soleymani, M. Hasanzadeh, N. Shadjou, M. Khoubnasab Jafari, J. V. Gharamaleki, M. Yadollahi, A. Jouyban, A new kinetic-mechanistic approach to elucidate electrooxidation of doxorubicin hydrochloride in unprocessed human fluids using magnetic graphene based nanocomposite modified glassy carbon electrode, *Materials Science and Engineering C* **61** (2016) 638-650. https://doi.org/10.1016/j.msec.2016.01.003
[30] L. Yang, L. Wang, K. Li, B. Ye, Sensitive voltammetric determination of neohesperidin dihydrochalcone based on SWNTs modified glassy carbon electrode, *Analytical Methods* **6** (2014) 9410-9418. https://doi.org/10.1039/C4AY02004A
[31] E. Laviron, General expression of the linear potential sweep voltammogram in the case of diffusionless electrochemical systems, *Journal of Electroanalytical Chemistry* **101** (1979) 19-28. https://doi.org/10.1016/S0022-0728(79)80075-3
[32] C. Li, Electrochemical determination of dipyridamole at a carbon paste electrode using cetyltrimethyl ammonium bromide as enhancing element, *Colloids and Surfaces B: Biointerfaces* **55** (2007) 77-83. https://doi.org/10.1016/j.colsurfb.2006.11.009

[33] B. Mekassa, P. G. L. Baker, B. S. Chandravanshi, M. Tessema, Sensitive electrochemical determination of ethambutol in pharmaceutical formulation and human urine at nickel nanoparticles/electrochemically reduced graphene oxide modified electrode, *Bulletin of the Chemical Society of Ethiopia* **33** (2019) 215-228. https://doi.org/10.4314/bcse.v33i2

[34] C. Bellei Perantoni, L. G. Soares Carbogim, F. Silva Semaan, R. Camargo Matos, D. Lowinsohn, Flow injection analysis of ethambutol in antituberculosis drugs using a graphite-paraffin electrode as amperometric detector, *Electroanalysis* **23** (2011) 2582-2585. https://doi.org/10.1002/elan.201100195

[35] C. B. Perantoni, A. B. R. de Azevedo, F. A. S. Vaz, M. A. L. de Oliveira, R. C. Matos, D. Lowinsohn, Flow injection analysis of ethambutol in synthetic urine using a graphite-polyurethane composite electrode as an amperometric detector, *Central European Journal of Chemistry* **11** (2013) 1668-1673. https://doi.org/10.2478/s11532-013-0301-9

[36] A. E. B. Lima, G. E. Luz Jr, N. C. Batista, E. Longo, L. S. Cavalcante, R. S. Santos, Determination of ethambutol in aqueous medium using an inexpensive gold microelectrode array as amperometric sensor, *Electroanalysis* **28** (2016) 985-989. https://doi.org/10.1002/elan.201500600

[37] R. F. Ngece, N. West, P. M. Ndangili, R. A. Olowu, A. Williams, N. Hendricks, S. Mailu, P. Baker, E. Iwuoha, A silver nanoparticle/poly (8-anilino-1-naphthalene sulphonic acid) bioelectrochemical biosensor system for the analytical determination of ethambutol, *International Journal of Electrochemical Science* **6** (2011) 1820-1834. https://doi.org/10.1016/S1452-3981(23)18149-1

[38] Z. Sepehri, H. Bagheri, E. Ranjbari, M. Amiri-Aref, S. Amidi, M. R. Rouini, Y. H. Ardakani, Simultaneous electrochemical determination of isoniazid and ethambutol using poly-melamine/electrodeposited gold nanoparticles modified pre-anodized glassy carbon electrode, *Ionics (Kiel)* **24** (2018) 1253-1263. https://doi.org/10.1007/s11581-017-2263-y

[39] R. A. S. Couto, M. B. Quinaz, Development of a Nafion/MWCNT-SPCE-Based portable sensor for the voltammetric analysis of the anti-tuberculosis drug ethambutol, *Sensors* **16** (2016) 1015. https://doi.org/10.3390/s16071015